Present tectonic motion across the Coast Ranges and San Andreas fault system in central California

Donald F. Argus*
Jet Propulsion Laboratory, California Institute of Technology, Pasadena, California 91109, USA

Richard G. Gordon†
Department of Earth Science, Rice University, Houston, Texas 77005, USA

ABSTRACT

Geodetic results from very long baseline interferometry (VLBI), satellite laser ranging (SLR), and the Global Positioning System (GPS) are used to estimate angular velocities between the Sierran microplate, Pacific plate, and North American plate. The Sierra-Pacific pole of rotation lies nearer to the San Andreas fault than does the Pacific–North America pole of rotation and leads to different tectonic implications than if the latter is used. The angular velocities show that the San Andreas fault system and central California Coast Ranges accommodate motion of 39 ± 2 mm/yr, mainly by strike-slip faulting. (All confidence limits following ± signs in this paper are 95% confidence limits.) Fault-normal motion is small, is mainly convergent (at rates up to 3.3 ± 1.0 mm/yr), and varies along the coast, but is divergent (at 2.6 ± 1.2 mm/yr) across San Pablo Bay and associated topographic lows across which the Sierran and Central Valley watershed drains to the Pacific Ocean. The mountain ranges tend to be larger where the fault-normal convergence rates are larger. The low convergence rate (0.5 ± 1.8 mm/yr) normal to the San Andreas fault in the Carrizo Plain differs sharply from that previously inferred (8.2 ± 1.2 mm/yr and 4.9 ± 1.6 mm/yr) by Feigl et al. (1993). The difference is due to differences between their and our elastic strain accumulation models and between how their and our Pacific plate reference frames are defined.

The ranges in most places require a minimum of 4 $^{+2}/_{-1}$ m.y. of fault-normal convergence at the present rate to attain their present cross-sectional area if erosion is neglected, more if it is not. The amount of convergence previously estimated from a balanced cross section across the Diablo Range in central California requires 10 $^{+8}/_{-3}$ m.y. of convergence at the present rate. The former is consistent with widely held views about the onset of the Coast Range orogeny, but the latter is not. Both are consistent, however, with the recent plate reconstructions by S. Cande, J. Stock, and colleagues, which indicate that Pacific plate motion relative to North America changed to a more convergent direction, 20°–25° clockwise of its prior direction, at ca. 8 to 6 Ma and not at 3.5 Ma, as had been previously inferred. The inferred change in direction of plate motion is large compared with the present angle of convergence across the straight and narrow segment of the San Andreas fault of 0.7°–4.7°, from which we infer that the Sierran microplate changed motion relative to North America at the same time (ca. 8 to 6 Ma) as did the Pacific plate. We further infer that the motion accommodated across the Great Basin must also have changed at the same time.

We also examine the hypothesis that stable sliding occurs along the San Andreas fault and other northwest-striking strike-slip faults in central California where the fault-normal convergence rate is low or negative, and that these faults are unstable where the fault-normal convergence rate is high. Such a relationship appears to hold in general, but fails in detail. In particular, there are substantial sections of fault with small inferred rates of fault-normal convergence across which the San Andreas fault is locked. Moreover, the creeping section of the San Andreas fault (i.e., the section between Parkfield and the Calaveras junction) is the locus of greater fault-normal convergence (3.2 ± 1.4 mm/yr) than is the locked part of the fault (0.5 ± 1.8 mm/yr) south of Parkfield. Thus, this hypothesis is at best a partial explanation for the observed distribution of locked and nonlocked sections of the fault.

Keywords: Calaveras fault, Coast ranges, Diablo range, San Andreas fault, San Francisco Bay, Sierra Nevada.

INTRODUCTION

The San Andreas fault system from its intersection with the Garlock fault to Point Arena is often described as being the Pacific–North American plate boundary, but it is more precisely described as the boundary between the Pacific plate and the Sierra Nevada–Great Valley microplate (hereinafter termed the Sierran microplate). The Sierran microplate in turn moves ~12 mm/yr relative to the North American plate (Argus and Gordon, 1991). This latter motion is mainly accommodated by deformation in the Great Basin and was first estimated by using geodetic measurements from VLBI (very long baseline interferometry) (Clark et al., 1987; Ward, 1988; Argus and Gordon, 1990, 1991; Gordon et al., 1993; Ma et al., 1994; Dixon et al., 1995) and more recently by using GPS (Global Positioning System) (Bennett et al., 1998; Thatcher et al., 1999; Dixon et al., 2000).

In this paper we use the assumption of the rigidity of plate interiors, a velocity model of plates and sites based on VLBI, SLR (satellite laser ranging), and GPS (Figs. 1 and 2, Table 1), the observed strike of the faults (Figs. 2 and 3, Table 2), and a slip budget for the faults (Figs. 3 and 4, Table 2) to

*E-mail: Donald.F.Argus@jpl.nasa.gov.
†rgg@rice.edu.

GSA Bulletin; December 2001; v. 113; no. 12; p. 1580–1592; 7 figures; 2 tables.

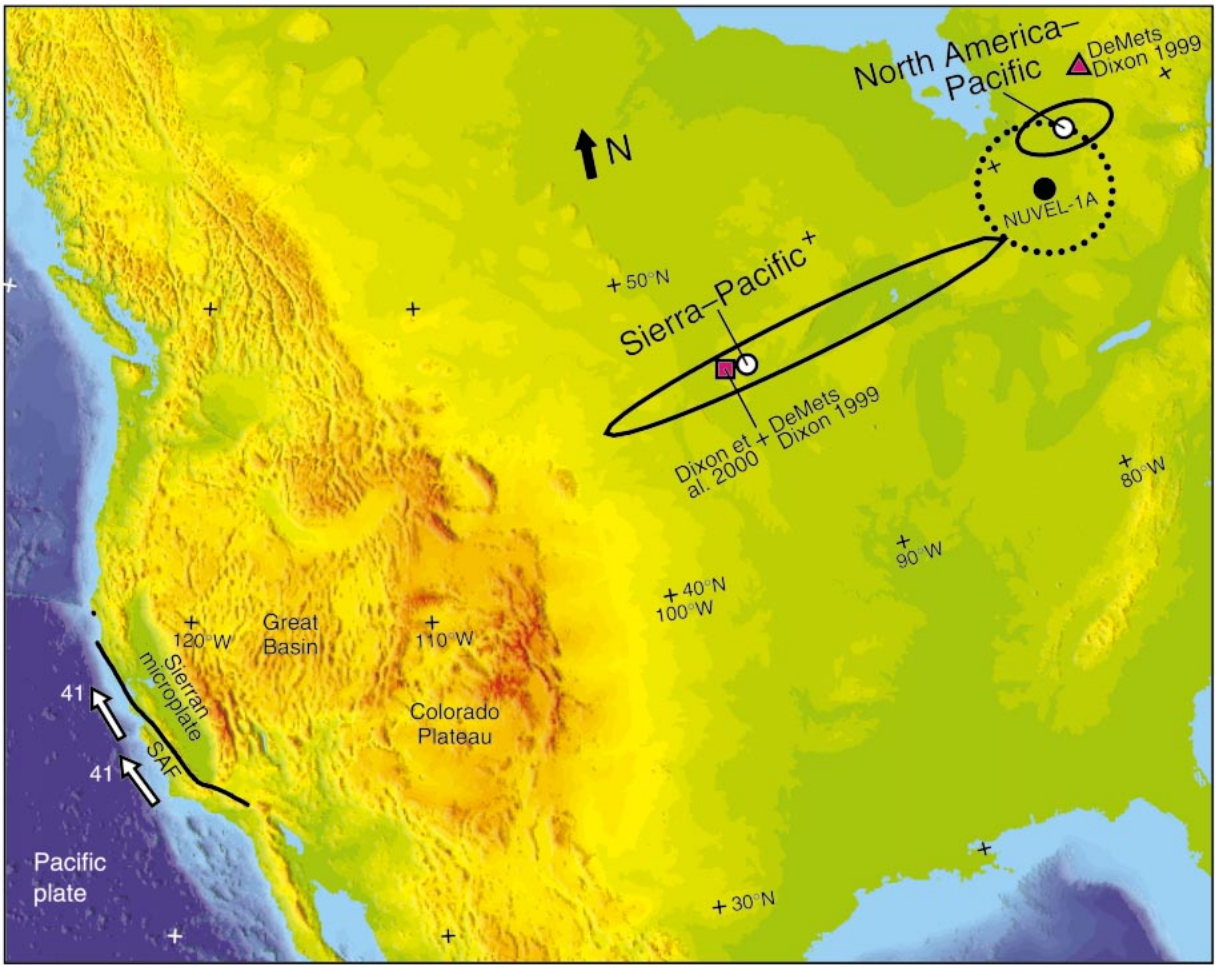

Figure 1. The Sierra-Pacific and North America–Pacific poles of rotation (white-filled circles) and 95% confidence limits (solid ellipsoids) determined in this study by using space geodesy are compared with (1) the NUVEL-1A North America–Pacific pole (black-filled circle) and 95% confidence limits (dotted ellipsoid), which are determined from transform-fault azimuths, earthquake slip vectors, and spreading rates from marine magnetic anomalies (DeMets et al., 1990, 1994), (2) the GPS North America–Pacific pole of DeMets and Dixon (1999), and (3) a GPS Sierra-Pacific pole (46.7°N, 95.6°W, 0.935°/m.y.) that we calculate by adding the Sierra–North America angular velocity of Dixon et al. (2000) to the North America–Pacific angular velocity of DeMets and Dixon (1999). This study's Sierra-Pacific angular velocity differs from the one inferred from Dixon's two articles by an insignificant 0.013°/m.y. Along the San Andreas fault at profile C–C′, our Pacific-Sierra velocity is 38.8 ± 1.7 mm/yr toward N38.1°W ± 2.6°, which is 0.9 mm/yr faster and 0.7° clockwise of that calculated from Dixon's two articles. This study's North America–Pacific angular velocity differs from the NUVEL-1A angular velocity by a marginally significant 0.040°/m.y. Along the San Andreas fault at profile C–C′, our Pacific–North America velocity is 49.5 ± 1.4 mm/yr toward N38.6°W ± 1.1°, which is 3.9 mm/yr faster and 2.1° counterclockwise of the NUVEL-1A prediction. Our Pacific-Sierra velocity is shown with the white-filled arrows west of the San Andreas fault (SAF); speeds are in mm/yr.

place kinematic constraints, not only on the tectonics of coastal California, but also on its along-strike variations. The along-strike variations are important for placing bounds on the long-term-average seismogenic potential of different regions of coastal California. We compare the predictions of the angular velocity of the Pacific plate relative to the Sierran microplate (Fig. 1) with the deformation across the Pacific-Sierra plate boundary (Figs. 2 and 3). This plate boundary includes not only the San Andreas fault and other similarly striking right-lateral strike-slip faults but also the folds and thrust faults that accommodate some of the wrenching and all of the fault-normal motion. It is this fault-normal motion that is responsible for raising the California Coast Ranges, which include the Temblor and Diablo Ranges, other ranges on the west flank of the Sacramento–San Joaquin Valley, and other ranges near the San Andreas fault system, as well as those strictly near the coast (Fig. 3). Prior results from local geodetic surveys have resolved the mainly fault-parallel shearing across the San Andreas and other subparallel strike-slip faults (Lisowski et al., 1991). Such surveys have typically been unable to resolve fault-normal motion (Lisowski et al., 1991), but recent detailed analyses of strain-accumulation rates in the San Francisco Bay area provide information on the horizontal strain tensor and its spatial variation (Savage et al., 1998). Here, we take a complementary approach: we use geodetic measurements from sites far from the deforming plate-boundary zone to estimate not only the fault-parallel but also the fault-normal components of velocity.

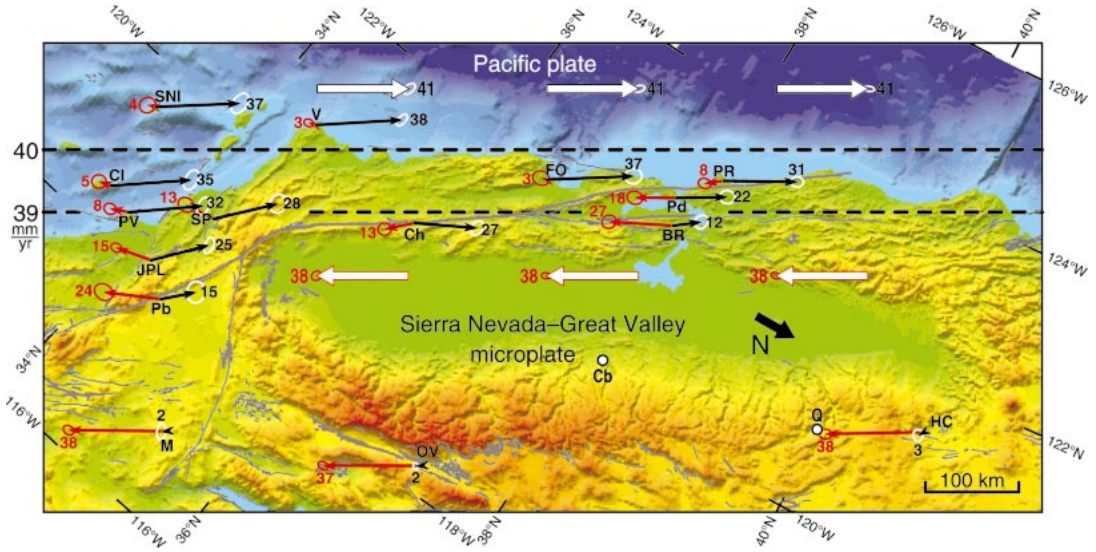

Figure 2. An oblique Mercator projection map about the Sierra-Pacific pole of rotation. The velocity of the Pacific plate relative to the Sierran microplate is horizontal everywhere in the projection. Two dashed horizontal lines serve as reference lines for relative speeds of 39 and 40 mm/yr. The wide, black-outlined, white-filled arrows depict the velocity of the Pacific plate relative to the Sierran microplate (i.e., the Sierra Nevada–Great Valley microplate); the narrow black arrows give the velocity of the individual sites relative to the Sierran microplate. The wide, red-outlined, white-filled arrows depict the velocity of the Sierran microplate relative to the Pacific plate; the narrow red arrows give the velocity of the individual sites relative to the Pacific plate. Error ellipses are 95% confidence limits. Site abbreviations: BR—Briones Reservoir, Ch—Carrhill, CI—Catalina Island, Cb—Columbia, FO—Fort Ord, HC—Hat Creek, JPL—Jet Propulsion Laboratory, M—Mojave, OV—Owens Valley Radio Observatory, Pb—Pearblossom, Pd—Presidio, PR—Point Reyes, PV—Palos Verdes, Q—Quincy, SNI—San Nicholas Island, SP—Santa Paula, V—Vandenberg Air Force Base. The velocities of the four sites (Vandenberg Air Force Base, Fort Ord, Presidio, and Point Reyes) in the upper fourth of the map were not used in estimating the angular velocity of the Pacific plate relative to the Sierran microplate. (SNI, CI, PV, SP, JPL, Pb, Ch, and BR also were not used.) Their velocities thus provide independent evidence of the direction of motion of coastal California relative to the Sierran microplate and of the net convergence relative to the San Andreas fault system implied by our calculations. Vandenberg, Fort Ord, Presidio, and Point Reyes move 2.1° counterclockwise, 1.0° counterclockwise, 0.2° counterclockwise, and 2.1° clockwise, respectively, of the calculated direction of plate motion. That the sites move nearly parallel to the direction of plate motion suggests that inferences from the Pacific plate velocity relative to the Sierran microplate are accurate. Because Vandenberg, Fort Ord, and Point Reyes are west of the San Andreas fault, the effect of elastic strain accumulation across the San Andreas fault causes their observed velocities relative to the Sierran microplate to be less than their long-term velocities (averaged over many earthquake cycles) relative to the Sierran microplate. Thus, for example, if the effect of elastic strain accumulation along any offshore faults is neglected, the long-term slip rate west of Vandenberg is at most 3 ± 2 mm/yr, whereas the long-term slip rate east of Vandenberg is at least 38 ± 2 mm/yr. Similarly, at most 8 ± 2 mm/yr of mainly plate-motion–parallel motion occurs west of Point Reyes, whereas at least 31 ± 2 mm/yr of motion occurs east of it. These bounds are consistent with the local trilateration data: Figure 15 of Lisowski et al. (1991) indicates that the geodetic network across the San Andreas system at Point Reyes measures total right-lateral strike slip of 31 mm/yr. At least 25 mm/yr occurs east and at least 1 mm/yr occurs west of Point Reyes.

TABLE 1. ANGULAR VELOCITIES

Plate pair	Lat (°N)	Long (°E)	ω (degrees m.y.$^{-1}$)	Major axis	Minor axis	Azimuth	Covariance Matrix					
							xx	xy	xz	yy	yz	zz
N. America–Pacific	50.1	−75.9	0.778 ± 0.014	1.6	0.7	97	220	64	−61	119	−68	108
Sierra–N. America	19.1	−138.6	0.243 ± 0.218	30.7	2.1	34	7097	12073	−11369	20759	−19514	18413
Sierra–Pacific	46.7	−94.6	0.930 ± 0.227	6.5	0.7	78	7338	12171	−11498	20695	−19498	18473

Note: Angular velocities correspond to right-handed rotations of the first named plate relative to the second. The major and minor axes, which are semiaxis lengths of the 95% confidence ellipse for the pole position, are given in great-circle degrees. ''Azimuth'' is the azimuth of the major semiaxis in degrees clockwise from north. The elements of the covariance matrix, which are given in Cartesian coordinates with the x axis through 0°N, 0°E, the y axis through 0°N, 90°E, and the z axis through 90°N, have units of 10^{-10} radians^2 m.y.$^{-2}$. The angular velocities of the plates and the velocities of sites relative to plates are estimated using a combination of three geodetic velocity solutions: (1) VLBI solution GLB1083c, which is determined from data from 1979 to 1997 (C. Ma and J. Ryan, Goddard Space Flight Center, 1997, electronic commun.), (2) SLR solution CSR96L01, which is determined from data from 1976 to 1996, (R. J. Eanes and M. M. Watkins, Center for Space Research, 1997, electronic commun.), and (3) a GPS solution determined from data from 1991 to October 1999 (M. B. Heflin, Jet Propulsion Laboratory, 2000, electronic commun.). The three solutions are analyzed using methods described in Argus and Gordon (1996) and Argus et al. (1999). The angular velocity of the Sierran microplate is estimated assuming that the motion of sites at Quincy and Columbia relative to the Sierran microplate is negligible and by using results from the trilateration network across Owens Valley (Savage et al., 1990) to estimate the motion of the Owens Valley radio telescope site relative to the Sierran microplate to be 2 ± 1 mm/yr toward S38°E ± 28°. The angular velocity of the Pacific plate is estimated from sites at Chatham island, Huahine, Kauai, Kwajalein, Marcus island, Maui, Mauna Kea, and Tahiti. The Sierra-Pacific pole of rotation is located 22.0° from the San Andreas Fault at profile C−C′, whereas the Pacific–North America pole of rotation is located 34.9° from the same point.

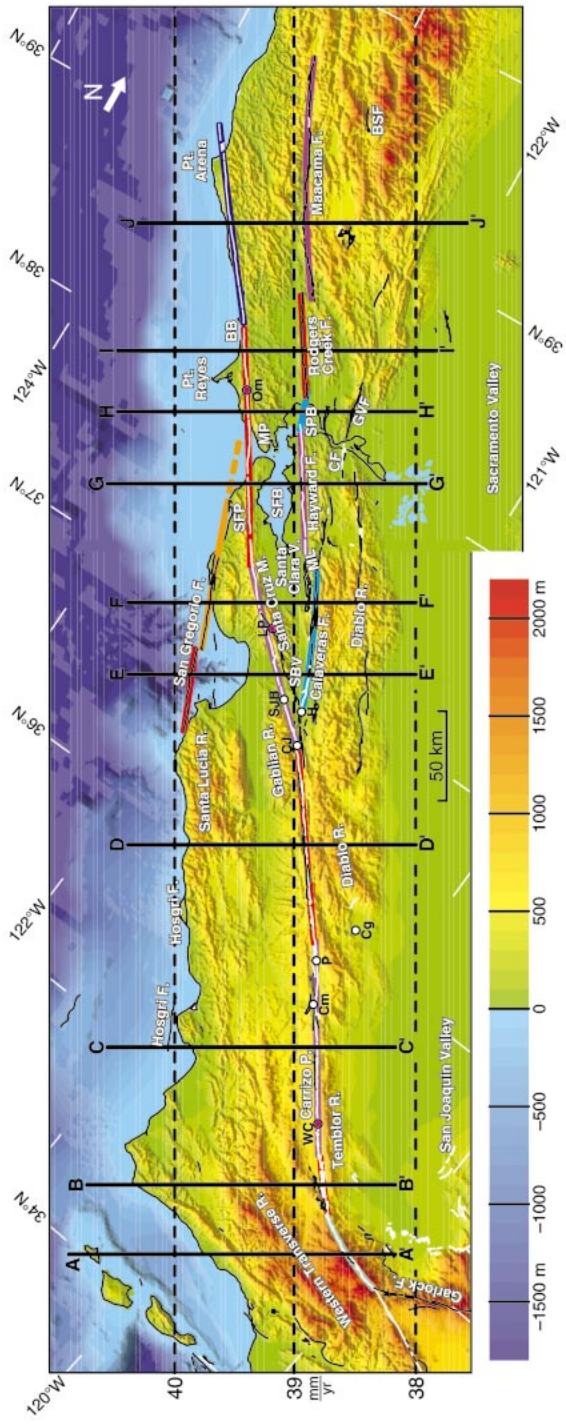

Figure 3. The direction of Pacific-Sierran plate motion is compared with the strikes of the main faults comprising the San Andreas fault system in this enlargement of the oblique Mercator projection. Colors indicate elevation. Small-circle segments (bold lines of various colors) are fit to the main Holocene (thin black) and historic (thin white) faults (Jennings, 1994). The amount of fault-normal convergence is calculated for the 10 profiles. Dashed parts of fault sections were not used in finding the small circle that best fits each section. Abbreviations: BB—Bodega Bay, BSF—Bird Spring fault, CF—Concord fault, Cg—Coalinga, CJ—Calaveras Junction, Cm—Cholame, GVF—Great Valley fault, H—Hollister, LP—Loma Prieta, ML—Mission link, MP—Monterey Peninsula, Om—Olema, P—Parkfield, SBV—San Benito Valley, SFB—San Francisco Bay, SFP—San Francisco Peninsula, SJB—San Juan Bautista, SPB—San Pablo Bay, WC—Wallace Creek.

MOTION OF THE PACIFIC PLATE RELATIVE TO THE SIERRAN MICROPLATE

The motion of the Pacific plate relative to the Sierran microplate is described in Table 1 and shown in Figures 2 and 3. The uncertainty in the direction of Pacific-Sierra motion varies between ±1.4° and ±3.1° (Table 2). (All confidence limits following ± signs in this paper are 95% confidence limits.) The relative speed indicated if all Pacific-Sierra motion were accommodated near Parkfield is 39 ± 2 mm/yr (Fig. 3). This speed is significantly faster than the Holocene slip rate estimated at Wallace Creek (Sieh and Jahns, 1984) of 34 ± 3 mm/yr, but insignificantly faster than the 38 mm/yr of right-lateral shear measured by a trilateration network near Hollister (i.e., the southeast Monterey Bay network shown in Fig. 13 of Lisowski et al., 1991). The plate velocity is significantly faster than the 25 mm/yr of right-lateral shear measured by a trilateration network across the Carrizo Plain, but the velocity gradient within the network suggests that additional motion is taken up outside the network (i.e., Fig. 12 of Lisowski et al., 1991). That these other estimates are consistently lower than the space geodetic rate estimate, and in at least one case significantly so, suggests that significant inelastic deformation occurs, that significant slip occurs on other faults such as the offshore Hosgri–San Gregorio fault, or that some combination of these phenomena occurs. Our Pacific-Sierra displacement rate of ~39 ± 2 mm/yr is consistent with the ~40 mm/yr slip rate across the San Andreas fault system that Freymueller et al. (1999) estimated by fitting a dislocation model of elastic strain accumulation to GPS observations north of San Francisco Bay.

If a straight line is drawn on Figure 3 to best fit the on-land trace of the San Andreas fault from about the middle of the Carrizo Plain (north of the big bend in the fault) to Point Arena in northern California, it strikes ~6° counterclockwise of the predicted direction of Pacific plate–Sierran microplate motion with most of the nonparallelness concentrated in the curved section between Hollister and the Santa Cruz Mountains. Therefore, the space geodetic data provide direct evidence that motion along the plate boundary cannot be purely strike slip and that some convergence is required across it, a conclusion previously inferred from combinations of space geodetic data and global plate-motion models (Minster and Jordan, 1987; Argus and Gordon, 1991) and from analysis of geologic structures, earthquake mechanisms, and bore-

TABLE 2. FAULT-PERPENDICULAR CONVERGENCE

Profile ID	Fault name	Fault-perp. convergence	Lat (°N)	Long (°E)	Fault strike	Plate motion direction
A–A′	San Andreas	20.7 ± 2.0	34.864	−119.180	−72.6	−40.1 ± 3.1
B–B′	San Andreas	5.0 ± 2.0	35.052	−119.556	−46.8	−39.4 ± 2.9
C–C′	San Andreas	0.5 ± 1.8	35.561	−120.106	−38.8	−38.1 ± 2.6
D–D′	San Andreas	3.2 ± 1.4	36.326	−120.905	−40.8	−36.1 ± 2.0
E–E′		2.2 ± 2.1				
	San Andreas		36.934	−121.656	−49.1	−34.5 ± 1.7
	Calaveras		37.017	−121.495	−26.0	−34.4 ± 1.7
	San Gregorio		36.690	−122.098	−26.8	−34.7 ± 1.6
F–F′		3.1 ± 1.8				
	San Andreas		37.180	−121.999	−46.9	−33.8 ± 1.6
	Calaveras		37.334	−121.708	−30.3	−33.6 ± 1.6
	San Gregorio		37.045	−122.264	−24.2	−33.9 ± 1.5
G–G′		0.4 ± 1.2				
	San Andreas		37.650	−122.464	−33.6	−32.6 ± 1.4
	Hayward		37.793	−122.180	−34.5	−32.4 ± 1.4
	San Gregorio		37.600	−122.561	−22.0	−32.7 ± 1.4
H–H′		−2.6 ± 1.2				
	San Andreas		37.949	−122.716	−33.8	−31.9 ± 1.4
	H.-R.C. relay		38.098	−122.415	−19.9	−31.7 ± 1.4
I–I′		1.8 ± 0.9				
	San Andreas		38.203	−122.933	−33.9	−31.3 ± 1.4
	Rodgers Creek		38.355	−122.616	−33.9	−31.1 ± 1.4
J–J′		3.3 ± 1.0				
	San Andreas		38.718	−123.427	−37.1	−30.1 ± 1.4
	Maacama		38.908	−123.010	−31.6	−29.8 ± 1.5

Note: Fault strike and plate motion direction are in degrees CW of north. The Pacific-Sierra velocity is computed using the geocentric coordinates of the Pacific-Sierra angular velocity and the geodetic coordinates of the locations along the faults. If the geodetic coordinates of fault locations were first converted to geocentric, then, for profile C−C′, the Pacific-Sierra azimuth would be 0.4° more counter-clockwise and shortening would be 0.24 mm/yr less. The quoted uncertainties include contributions from (i) the uncertainty in the speed of Pacific-Sierra plate motion, (ii) the uncertainty in the azimuth of Pacific-Sierra plate motion, (iii) the uncertainty in the slip rate along the East Bay faults [applicable to profiles E−E′ thru J−J′], and (iv) the uncertainty in the slip rate along the San Gregorio fault [applicable to profiles E−E′, F−F′, and G−G′]. (i) is much smaller than (ii) for all profiles. (ii) is the largest for all profiles except for profiles F−F′ and G−G′, at which (i), (ii), and (iii) are largest and about the same size.

hole-breakout data (Page and Engebretson, 1984; Zoback et al., 1987; Mount and Suppe, 1987; Namson and Davis, 1988; Jamison, 1991).

Although the San Andreas is clearly the dominant fault trace south of the San Benito Valley, where the Calaveras fault begins in a right stepover from the San Andreas, the transform system north of there consists of multiple strike-slip faults composing a broad zone of deformation (Fig. 3). If, instead of the San Andreas, one or more of these other branches is followed north of the junction with the Calaveras fault (hereinafter termed ''Calaveras junction,'' see Fig. 3), the difference from the direction of plate motion is much smaller. For example, taken together, five fault segments lie nearly along a single small circle centered on the pole of rotation between the Pacific plate and the Sierran microplate. These five sections are (1) the sections of the San Andreas north of the big bend in the fault and south of the Calaveras junction, (2) the southern two-thirds of the Calaveras fault, (3) the Hayward fault, (4) the Rodgers Creek fault, and (5) the Maacama fault. These combined sections have an average angle that differs insignificantly (~1° counterclockwise) from the direction of motion of the Pacific plate relative to the Sierran microplate. Although Page (1984) concluded that motion on the Calaveras fault zone began after 3.6 Ma, newer work and interpretation indicate that the Calaveras and other East Bay faults initiated at ca. 8 Ma (McLaughlin et al., 1996). Therefore, the inferred fault-normal convergence rate is, and has been, much smaller than the rate that would be estimated if only the San Andreas fault is considered.

FAULT-NORMAL CONVERGENCE RATES

Method

The rate of fault-normal convergence was estimated on 10 great-circle profiles normal to Pacific-Sierra motion (Fig. 3). The southernmost profile crosses the western Transverse Ranges and the big bend of the San Andreas fault and the northernmost profile crosses the San Andreas fault system south of Point Arena. Across the four profiles south of the Calaveras junction (Fig. 3), estimation of fault-normal convergence and its uncertainty is straightforward if one assumes that all strike slip is taken up along the San Andreas fault itself. The estimated convergence rate and uncertainty is simply the projection of the Pacific-Sierra velocity onto the fault-normal direction. The much smaller amount of slip possibly taken up on the Hosgri and other faults that are subparallel to the San Andreas would only very modestly alter estimates of fault-normal convergence.

Estimation of fault-normal convergence across the six profiles north of the Calaveras junction is more complicated, however, because the slip is divided between the San Andreas fault and faults east of the Santa Clara Valley and San Francisco Bay. How much of the slip is taken up along the San Andreas itself and how much is taken up along the faults to the east is uncertain, but any set of estimated slip rates must sum to the total Pacific-Sierra velocity (Fig. 4).

The estimated fault-normal convergence also depends on the unknown motion of the crust east of the San Andreas fault but west of the East Bay faults. We calculate the fault-normal convergence for two limiting cases for the motion of this intervening crust (Fig. 4). First, we assume that the motion between this block and the Pacific plate parallels the San Andreas fault. Second, we assume that the motion between this block and the Sierran microplate parallels the fault assumed to be active east of the San Andreas. Figure 4 shows this calculation for profile E–E′ and shows that the rate of convergence assuming no convergence across the San Andreas fault differs by only 0.19 mm/yr from that assuming no convergence across the Calaveras fault. The true answer must lie between these two estimates because the shortening is in fact widely distributed. In Table 2 and elsewhere we have given the mean of the two estimates.

Slip Budget and Bounds on Slip Rates

To formulate our slip budget for faults north of the Calaveras Junction, we use several constraints that place lower bounds and upper bounds on the slip rate. Because Fort Ord is west of the San Andreas fault, the effect of elastic strain accumulation across the San Andreas fault causes its observed velocities relative to the Sierran microplate to be less than its long-term velocities (averaged over many earthquake cycles) relative to the Sierran microplate. We assume that the elastic strain accumulation at Fort Ord from the San Andreas fault is larger than that from the Hosgri–San Gregorio fault because of the presumably much faster slip rate of the former relative to the latter. Therefore, the long-term slip rate west of Fort Ord is at most 3 ± 3 mm/yr in the plate-motion–parallel direction, whereas

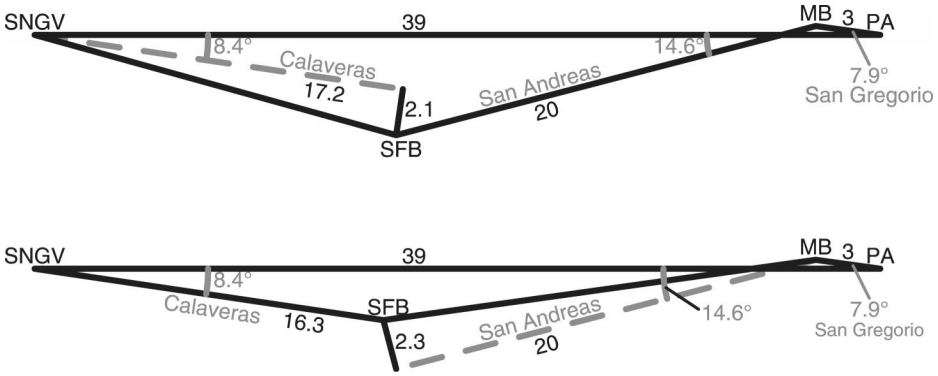

Figure 4. Velocity space representation of velocities across profile E–E′. The strike of the San Andreas fault across this profile is 14.6° counterclockwise of the velocity of the Pacific plate relative to that of the Sierran microplate (SNGV), the strike of the Calaveras fault is 8.4° clockwise of the same velocity, and the strike of the San Gregorio is 7.9° clockwise of the velocity. In the solution at the top, the motion of the Santa Clara Valley–San Francisco Bay block (SFB) relative to the Monterey Bay block (MB) parallels the San Andreas fault, which slips at 20 mm/yr, and the motion of the Monterey Bay block relative to the Pacific plate (PA) parallels the San Gregorio fault, which slips at 3 mm/yr. The difference vector between the Pacific-Sierra velocity and the velocities assumed along the San Andreas and San Gregorio faults is then resolved into components parallel and perpendicular to the Calaveras fault, the former being the estimate of the slip rate along the Calaveras, which is 17.2 mm/yr, and the latter being the estimate of fault-normal convergence, which is 2.1 mm/yr. In the solution at the bottom, the motion of the Santa Clara Valley–San Francisco Bay block (SFB) relative to the Sierran microplate (SNGV) parallels the Calaveras fault, which slips at 16.3 mm/yr, and the motion of the Monterey Bay block (MB) relative to the Pacific plate (PA) again parallels the San Gregorio fault, which again slips at 3 mm/yr. The difference vector between the Pacific-Sierra velocity and the velocities assumed along the Calaveras and San Gregorio faults is then resolved into components parallel and perpendicular to the San Andreas fault, the former being the estimate of the slip rate along the San Andreas, which is 20 mm/yr, and the latter being the estimate of fault-normal convergence, which is 2.3 mm/yr.

motion east of Fort Ord is at least 37 ± 3 mm/yr (Fig. 2). We use the former estimate to bound slip along the San Gregorio fault.

VLBI data give a lower bound on the combined rate of slip of the San Andreas and San Gregorio faults along the San Francisco Peninsula. The Presidio VLBI radio telescope site lies east of the San Andreas fault and is closer to the San Andreas than to the East Bay faults (Fig. 2). Because the San Andreas is probably slipping faster than are the East Bay faults, and because the San Andreas along the San Francisco Peninsula is locked whereas the East Bay faults are creeping, the site is surely more strongly influenced by elastic strain accumulation across the San Andreas than across the East Bay faults. Thus, the site's observed motion gives an upper bound of 22 ± 3 mm/yr on the long-term rate of motion across faults east of the San Andreas. At the same time at least 18 ± 3 mm/yr of motion must be taken up across the San Andreas and faults west of it.

A greater lower bound is provided by a minimum Holocene rate of slip along the San Andreas of 24 ± 3 mm/yr (which we take to be a 95% confidence limit) from trenching at the Wind Gap site near Olema, 45 km north of San Francisco (Niemi and Hall, 1992). Olema (labeled Om) is between profiles H–H′ and I–I′ in Figure 3. As the Wind Gap (i.e., Olema) site lies north of where the San Gregorio fault joins the San Andreas fault near Bolinas Lagoon, the implied minimum slip rate of 21 mm/yr applies to the sum of San Andreas and San Gregorio slip along the San Francisco Peninsula and is the greatest lower bound available for that sum.

Upper bounds on the San Andreas (plus San Gregorio) slip rate are also available from both geologic and geodetic data. A trenching investigation farther north along the San Andreas, near Point Arena, indicates a 25 ± 3 mm/yr maximum slip rate (Prentice, 1989). A lower upper bound on the rate of San Andreas slip can also be inferred from geodetic data. Examination of Figure 13 of Lisowski et al. (1991) indicates that strain accumulating along the East Bay faults south of San Francisco Bay is at least 19 ± 3 mm/yr. Performing a vector subtraction of this slip rate from the Pacific-Sierra plate rate and then propagating errors leaves 20.7 ± 4.3 mm/yr as the maximum slip rate along the San Andreas plus San Gregorio. The uncertainty, ±4.3 mm/yr, is derived from adding in quadrature the ±3 mm/yr uncertainty in Calaveras slip rate and the ±3 mm/yr uncertainty in rate between the Pacific plate and the Sierran microplate.

Together these constraints limit the combined slip on the San Andreas and San Gregorio faults to 21–25 mm/yr. Using symmetric confidence limits gives a slip rate of 23 ± 2 mm/yr for this combined slip rate north of the Calaveras junction; we assume that the rest of the slip occurs on the eastern faults. The partitioning of the slip on the strike-slip faults of central and northern California is surely more complex than this simple budget, in particular because there is not a single fault but multiple faults east of the San Andreas. Across most profiles, however, these eastern faults have similar strikes (Fig. 3), and their incorporation into a more complex model of slip budget would only modestly alter our estimates of fault-normal convergence. For profiles E–E′, F–F′, and G–G′, however, the strike of the San Gregorio fault differs significantly from that of the San Andreas fault. We have thus included slip of 3 ± 3 mm/yr, as already explained, on the San Gregorio fault (and reduced the San Andreas slip by the same amount) to obtain the fault-normal convergence rate across these three profiles.

Differences from the Model of Feigl et al. (1993)

We obtain results that differ significantly from those of Feigl et al. (1993). In particular, we infer rates of fault-perpendicular convergence near the Carrizo plain section of the San Andreas fault much lower than their estimates, as is discussed soon. There are two main differences in how Feigl et al.'s (1993) estimate and our estimate of convergence were calculated. First, we simply present the velocities without correction for any a priori model for how motion is accommodated across the boundary between the Pacific plate and the Sierran microplate, whereas Feigl et al. (1993) constructed a model for the velocities due to elastic strain accumulation along the San Andreas fault system, which they subtracted from their observed site velocities. When we construct a model for elastic strain accumulation, we find values for the modeled velocities that are very different from theirs and that would

only modestly affect our estimates of convergence. The correction implied by their model accounts for about four-fifths of the difference between their results and ours. Second, the frame of reference in which the velocities are described differ. Here, our velocities are described relative to a fixed Pacific plate frame of reference, which is determined from geodetic observations on Pacific plate islands far from the California coast. On the other hand, Feigl et al. (1993) used no geodetic observations from sites in the Pacific plate interior. Instead they first estimated velocities relative to a reference frame fixed to North America. They then used a rescaled version of the NUVEL-1 Pacific–North America angular velocity, which is based on spreading rates determined from marine magnetic anomalies, the orientation of submarine transform faults, and the orientation of slip vectors from earthquakes that occur along plate boundaries (DeMets et al., 1990), to transform their set of velocities from the North American to the Pacific frame of reference. Because the rescaled NUVEL-1 angular velocity differs from the one that best fits the geodetic data, their indirectly inferred Pacific frame of reference rotates relative to our directly inferred frame of reference and accounts for about one-fifth of the difference between their model and ours. Thus, we conclude that their high estimate of convergence is a consequence not of the geodetic observations but mainly of their elastic strain accumulation model and partly of the rotation of their Pacific plate frame of reference.

Results

We find that the rate of fault-normal convergence is smaller than nearly all prior estimates (Table 2). For example, Harbert (1991) concluded that the present convergence is due to a 12° clockwise change in motion of the Pacific between 4 and 3 Ma, which would imply a convergence rate of ~10 mm/yr along the entire California coast. In contrast, we find rates of fault-normal convergence no larger than 3.3 ± 1.0 mm/yr except for the two profiles, A–A′ and B–B′, across the big bend section of the San Andreas (Table 2). Across some sections of the fault system (profiles C–C′ and G–G′), the estimated fault-normal convergence rate does not differ significantly from zero. Moreover, across the northern San Francisco Bay region, the fault-normal convergence rate is significant and negative—we find fault-normal divergence on profile H–H′ and small fault-normal convergence on nearby profiles G–G′ and I–I′. Results for specific regions are described next.

Southern Curved or Big Bend Section of the San Andreas Fault

Deformation is distributed both northeast and far to the southwest of the big bend section of the San Andreas fault. The inferred convergence rate across A–A′ of 20.7 ± 2.0 mm/yr greatly exceeds the fault-normal convergence rate inferred anywhere to the north. Convergence is slower (5.0 ± 2.0 mm/yr across profile B–B′) in the transitional section between the big bend section and the Carrizo Plain section.

Carrizo Plain Section of the San Andreas Fault

The simplest part of the San Andreas fault system is north of the big bend in the fault and south of the Calaveras junction (Fig. 3). The plate velocity nearly parallels this straight section of the fault (Fig. 3, Table 2). Across profile C–C′, we infer a fault-normal convergence rate of 0.5 ± 1.8 mm/yr and thus an upper bound of 2.3 mm/yr. This small upper limit on convergence rate is smaller than the 5 mm/yr limit that we found before from fewer data (Argus and Gordon, 1991) and is consistent with the insignificant amount of shortening normal to the fault observed in trilateration networks spanning the fault (Lisowski et al., 1991).

Our new result disagrees sharply, however, with some of the results of Feigl et al. (1993), who estimated 8.2 ± 1.2 mm/yr of fault-normal convergence between the radio telescope at Owens Valley and the interior of the Pacific plate and 4.9 ± 1.6 mm/yr of fault-normal convergence between the GPS site at Buttonwillow (in the San Joaquin Valley) and the Pacific plate. Neither of these estimates is consistent with the 0.5 ± 1.8 mm/yr of fault-normal convergence we estimate between the Pacific plate and the Sierran microplate along profile C–C′.

Southern Diablo Range Section of the San Andreas Fault

Farther north, across the section lying between Parkfield and Hollister (profile D–D′ in Fig. 3), the fault-normal convergence rate is 3.2 ± 1.4 mm/yr. Although higher than for the Carrizo Plain, the convergence rate is still consistent with the dominance of shearing parallel to the San Andreas indicated by results from geodolite networks across the fault system (Lisowski et al., 1991). Our new limits on convergence rate are both consistent with, and provide tighter limits than, the previously estimated 5.7 ± 5.3 mm/yr of convergence along N16°E (Sauber et al., 1989). When projected onto the fault-normal direction of N49°E, this convergence rate is 4.8 ± 4.4 mm/yr, which gives a 95% confidence interval of 0.4–9.2 mm/yr—which contains our 95% confidence interval of 1.8–4.6 mm/yr.

Sections North of the Calaveras Junction

The section of the San Andreas fault from the Calaveras junction through the Santa Cruz Mountains strikes ~15° counterclockwise of the direction of Pacific plate–Sierran microplate motion (profiles E–E′ and F–F′ in Fig. 3 and Table 2), whereas the Calaveras and San Gregorio faults both strike 3°–10° clockwise of the direction of plate motion (Fig. 3, Table 2). The rates of fault-normal convergence are 2.2 ± 2.1 mm/yr for profile E–E′ and 3.1 ± 1.8 mm/yr for profile F–F′.

Sections from San Francisco Bay to Bodega Bay

Across profile G–G′, which crosses the San Francisco Peninsula, the strikes of the San Andreas fault and Hayward faults are slightly counterclockwise of the inferred plate velocity, but the strike of the San Gregorio fault is clockwise of the inferred plate velocity. These directions combine to give a small, insignificant net convergence rate (Fig. 3, Table 2). Across profile H–H′, which crosses the Marin Peninsula and San Pablo Bay, the strike of the San Andreas fault is slightly counterclockwise of the inferred plate velocity, but the inferred average strike of the extensional relay that connects the Hayward fault with the Rodgers Creek fault is clockwise of the inferred plate velocity, and these directions combine to give a small, significant net divergence (Fig. 3, Table 2). Across profile I–I′, which intersects the coast between Point Reyes and Bodega Bay, the strikes of the San Andreas fault and the Rodgers Creek fault are slightly counterclockwise of the inferred plate velocity, which combine to give a small net convergence rate (Fig. 3, Table 2).

Profiles F–F′, G–G′, and H–H′ cross a network of San Francisco Bay area trilateration observations analyzed by Savage et al. (1998). The results of our analysis provide an interesting transition from south to north from highly significant fault-normal convergence (3.1 ± 1.8 mm/yr along profile F–F′) across the Santa Cruz Mountains and the Diablo Range near their locally maximum extent (Figs. 3 and 5), through insignificant convergence (0.4 ± 1.2 mm/yr along profile G–G′) across modestly elevated terrain, to significant divergence (–2.6 ± 1.2 mm/yr along profile

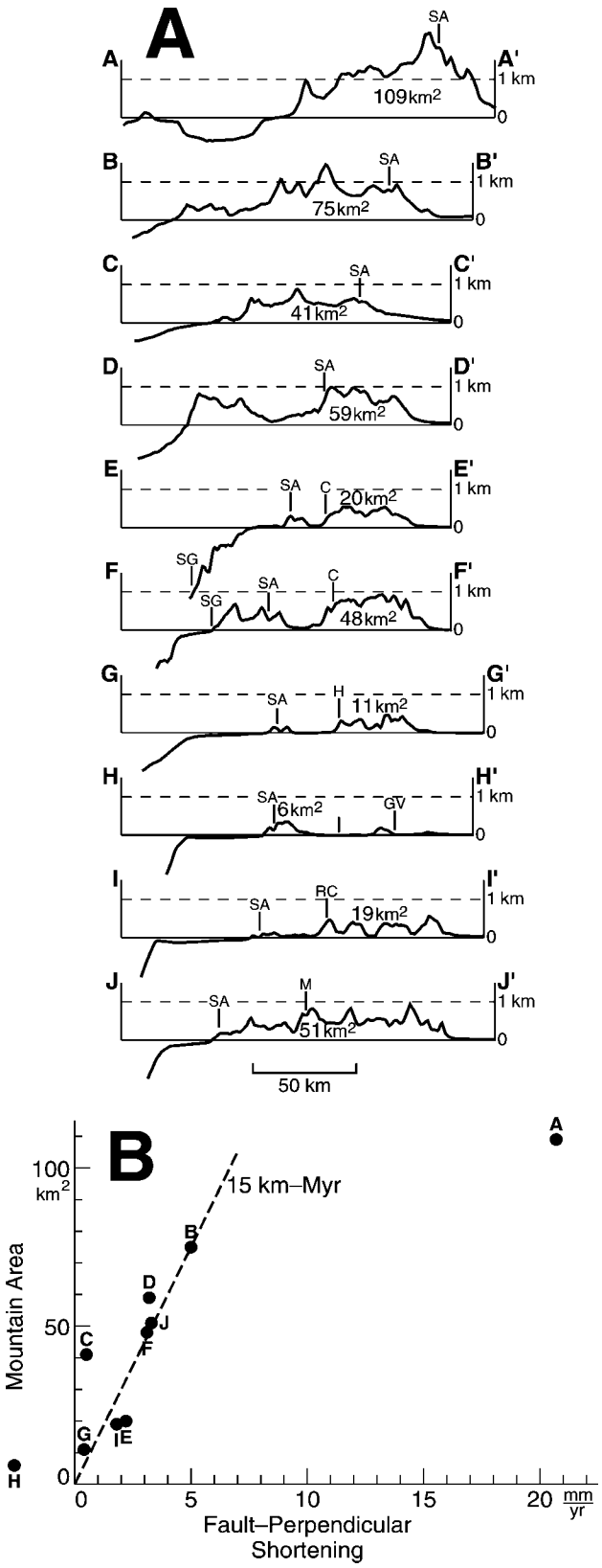

Figure 5. (A) Topographic profiles along the 10 great-circle segments in Figure 3. Each great-circle segment is normal to the direction of Pacific-Sierra plate motion. The area above sea level along each profile is given. Vertical exaggeration is 19:1. (B) Cross-sectional area normal to the direction of plate motion of the California Coast Ranges (from profiles A–J in part A) vs. the rate of fault-normal convergence. Dashed line has a slope of 15 km•m.y.

H–H′) across terrain of negligible elevation that includes a presumably active pull-apart basin in San Pablo Bay. Savage et al. (1998) presented several parameters over a grid of 32 polygons that covers their entire San Francisco Bay area network. None of these parameters is precisely the same quantity that we estimate here, but the values and spatial distribution of two of their parameters are usefully compared with our results. The first of these is the extension rate along N58°E, which is perpendicular to the direction of Pacific-Sierra motion. There is a weak tendency in their network for contraction to be larger (or in some cases extension to be smaller) in the southern part of their network, a tendency that is in qualitative agreement with the results we present here. Second, their map of spatial distribution of dilatation indicates a region of negative dilatation (i.e., areal contraction) concentrated in the Santa Cruz Mountains and Santa Clara Valley spanned by profile F–F′. Moreover, the 6236 km^2 area of their southern subnetwork apparently decreased in area by an insignificant 19 ± 130 m^2/yr (Savage et al., 1998), in qualitative agreement with our estimation of significant fault-normal convergence along F–F′. In their northern subnetwork, however, the 5989 km^2 area increased by 231 ± 180 m^2/yr (Savage et al., 1998), in qualitative agreement with our finding of insignificant fault-normal convergence along G–G′ and significant fault-normal divergence along H–H′.

Bodega Bay to Point Arena

Across profile J–J′, which intersects the coast between Bodega Bay and Point Arena, the strike of the San Andreas fault is distinctly counterclockwise, and the Maacama fault is slightly counterclockwise of the inferred plate velocity, which combine to give the largest net convergence rate outside of the big bend region (Fig. 3, Table 2).

FAULT-NORMAL CONVERGENCE RATE AND THE SIZE OF THE COAST RANGES

Mountains presumably are a consequence of horizontal shortening of the crust and perhaps the lithospheric mantle as well. Figure 3, combined with the fault-normal convergence rates of Table 2, indicates that there is a good qualitative correlation in location between the present rate of fault-normal convergence and the size and extent of the nearby coastal ranges. This relationship is further explored in Figure 5. Figure 5A shows the topographic profiles along the 10 great-circle segments of

Figure 3. We take the cross-sectional area above sea level to be a simple objective measure of the size of the mountains along a profile. These values are indicated in Figure 5A and are plotted versus the fault-normal convergence rate in Figure 5B, which lends further support to the correlation, especially for the ranges east of the fault (Fig. 5A). In particular, the size of the Coast Ranges east of the fault are moderate near San Pablo Bay, San Francisco Bay, and along the Carrizo Plain (i.e., adjacent to the Temblor Range) where the fault-normal convergence rates are only 0.4 ± 1.2 mm/yr and 0.5 ± 1.8 mm/yr, respectively. On the other hand, the Diablo Range, which is a higher and wider range, flanks sections with fault-normal convergence rates of 2.2 ± 2.1 mm/yr to 3.1 ± 1.8 mm/yr. Moreover, extensive ranges west of the Sacramento Valley flank sections with fault-normal convergence of 3.3 ± 1.0 mm/yr (Figs. 3 and 5).

The goodness of this correspondence is a little surprising because the convergence rate reflects instantaneous motion, whereas the mountain ranges have formed by shortening over millions of years. Moreover, prior to the northwestward passage of the Mendocino triple junction, coastal California was the site not of slightly convergent wrenching, but of oblique convergence, as the Farallon or Juan de Fuca plate was subducted beneath California. Therefore, some of the mountains, especially those not far south of the present triple junction near Cape Mendocino are at least partly relicts of an earlier episode of convergence like that now presumably raising the coastal mountains east and north of Cape Mendocino. Moreover, some excess height, decreasing with distance southeastward from Mendocino triple junction, has been inferred to be caused by hot mantle that fills a gap left in the wake of the migrating Mendocino triple junction (Furlong, 1993).

Complexities are expected also in the southeastern part of Figure 3, particularly for profiles A–A′, B–B′, and C–C′. For example, mountains are now being raised on the west side of the San Andreas fault adjacent to the big bend section presumably because of the very large fault-normal convergence implied there. These mountains are being transported with the Pacific plate at ~39 mm/yr to the northwest and may later flank the San Andreas along sections where little or no fault-normal convergence occurs today.

The strength of the correlation mainly depends, however, on the points corresponding to profiles D–D′, F–F′, and J–J′. Given that the mountains on these profiles are dominantly east of the San Andreas fault, they formed in place in a reference frame fixed to the Sierran microplate. Consequently, their interpretation is simpler than might otherwise be the case.

STRIKE-SLIP MOTION COMPARED WITH FAULT-PARALLEL PLATE MOTION

The 39 ± 2 mm/yr fault-parallel component of plate motion significantly exceeds the 34 ± 3 mm/yr Holocene slip rate estimated at Wallace Creek in the Carrizo Plain segment of the fault. The difference between these two rates, 5 ± 4 mm/yr, must be accommodated by inelastic deformation, by slip along other (possibly offshore) faults, or both. Here we examine how much of this might be accommodated by inelastic deformation.

Jamison (1991) presented kinematic models for contractional fold development in wrench and convergent-wrench terranes. His models relate fold shortening, axial rotation, and axial extension. He used observed fold geometry and axial orientation to determine fold shortening and axial extension, which can be resolved into components of shearing parallel to, and components of convergence perpendicular to, the San Andreas fault. His analysis shows that the folds adjacent to the fault in the Temblor Range are the result of strongly convergent wrenching. He estimated shortening perpendicular to the folds to be between 4% and 14%, which we take to be a 95% confidence interval, and extension parallel to the fold axis to be between 1% and 4.5%. The resulting displacements resolve into components of integrated shearing parallel and convergence perpendicular to the San Andreas fault of 5.3 ± 3.2 km and 6.4 ± 3.8 km, respectively. If the integrated shearing has occurred at a constant rate over, for example, the past 6 m.y., inelastic deformation adjacent to the Carrizo section of the San Andreas gives a fault-parallel displacement rate of only 0.9 ± 0.5 mm/yr. By itself, it is sufficient to reduce the 5 ± 4 mm/yr difference between the plate rate and the fault-slip rate at Wallace Creek to an insignificant 4 ± 4 mm/yr. A larger part of the difference may be due, however, to shear strain that occurred by penetrative ductile flow that produces neither faults nor folds. Jamison (1991) cited physical models in which such shear strain may be as large as 30% to 40%. Insofar as this is true for the region adjacent to the San Andreas fault, the 5 ± 4 mm/yr shortfall, which corresponds to a fault-parallel displacement of 30 ± 24 km if it has persisted for 6 m.y., is readily accommodated. For example, if this shear strain is accommodated over 85 km, the same width over which folding is observed to occur, the strain would be 35% ± 28%, similar to the amount observed in some physical models.

TOTAL CONVERGENCE AND TIMING OF THE COAST RANGE OROGENY

We next use eight of the topographic profiles of Figure 5 and a simple model for isostatic compensation to obtain minimum estimates of the total convergence across the Coast Ranges. We exclude profile A–A′ because it is across the Transverse Ranges, not the Coast Ranges, and we exclude profile H–H′ because there is divergence, not convergence, across it.

England and Houseman (1989) showed that for a wide variety of assumptions, the change in elevation, Δe, is approximately proportional to the change in crustal thickness, Δs. Let that constant of proportionality be denoted by B, which gives

$$\Delta e = B\,\Delta s. \tag{1}$$

We are interested in the elevation change not at a single location but along an entire profile across the Coast Ranges. Thus, we wish to relate

$$\Delta E = \int \Delta e\, dx \text{ to}$$

$$\Delta S = \int \Delta s\, dx,$$

where ΔE is the integral of the change in elevation across a profile and ΔS is the integral of the change in crustal thickness in an area. It follows that

$$\Delta E = B\,\Delta S. \tag{2}$$

Thus, if we know B, we can estimate ΔS given the observed ΔE. For a model of Airy isostasy in which the crust but not the lithospheric mantle is thickened by fault-normal convergence, the constant of proportionality B is given by

$$B = (\rho_m - \rho_c)/\rho_m. \tag{3}$$

Taking ρ_c to be 2700 kg·m^{-3} and ρ_m to be 3200 kg·m^{-3} gives a value for B of 0.156. If instead it is also assumed that the lithospheric mantle thickens along with the crust, B would be smaller (England and Houseman, 1989) and our estimated value of convergence would be larger. Because the lithospheric mantle be-

neath coastal California is relatively thin, with total lithospheric thickness from 30 to 60 km, much thinner than the 120 km to 170 km thickness observed in the central and eastern United States (Fuis and Mooney, 1990), the Airy model may only modestly overestimate the value of *B.* In any event, neglecting the effect of thickening of the lithospheric mantle causes our estimate of ΔS to be a minimum estimate, as does our neglect of the effect of erosion.

The amount of convergence, *C,* is related to ΔS by

$$C = (\Delta S)/h_c, \qquad (4)$$

where h_c is the crustal thickness before horizontal convergence began. The present crustal thickness from the Carrizo Plain to Point Arena in central California increases eastward from ~23 km near the coast to ~28 km beneath the Diablo Range; a typical value near the San Andreas fault is ~25 km (Fuis and Mooney, 1990). The crust was surely thinner before the onset of the Coast Range orogeny than it is now, but for the purposes of our calculation, we take the crustal thickness to be 25 km. Because this is a maximum estimate of initial crustal thickness, it will cause our estimate of convergence (Fig. 6) to be a minimum. That ΔS is also a minimum, as already discussed, also causes our estimate of convergence to be a minimum.

Two published estimates of convergence can be compared with the convergence we estimate here. Namson and Davis (1988) estimated late Cenozoic convergence across the California Coast Ranges to be 33 km on a profile near our profile D–D′ (Figs. 3 and 6). Their estimate is greater than the 15 km minimum convergence we estimate across D–D′ (Fig. 6).

As already discussed, Jamison (1991) estimated the fault-normal convergence across the Temblor Range manifested by folding adjacent to the San Andreas fault to be 6.4 ± 3.8 km, well below the estimate we show in Figure 6 for profile C–C′, which is the most appropriate for comparison with his result. We are encouraged by this, however. The convergence for profile C–C′ is a poor fit to the straight line that best fits the rest of the points shown in Figure 6. Moreover, unlike profiles farther north, most of the elevation lies west of the San Andreas on crust that would have been in the big bend region at just 1–2 Ma.

The slope of a straight line fit through the origin of Figure 6 has the dimensions of time and corresponds to the time needed to build the mountains to the observed size. For reference, we show three straight (solid) lines corresponding to time intervals of 3 m.y., 6 m.y., and 9 m.y. If the ranges were built in just the past 1–3 m.y., as is widely believed, all the points should fall below the line labeled ''3 m.y.,'' and two of them (E and I) do. Six points lie above the line, indicating greater minimum durations. Point C, already discussed, is inconsistent with the shortening estimated by Jamison (1991), and we will consider it no further. Points G, F, J, and B are consistent with the 3 m.y. line when the uncertainty in fault-perpendicular convergence rate is considered. All four points are consistent with a minimum duration of $4^{+2}/_{-1}$ m.y. Point D requires a minimum duration of slightly more than 3 m.y. The estimate of convergence from balanced cross sections near profile D (Namson and Davis, 1988) is much greater than that inferred from topography and indicates that $10^{+8}/_{-3}$ m.y. is required to attain the observed convergence.

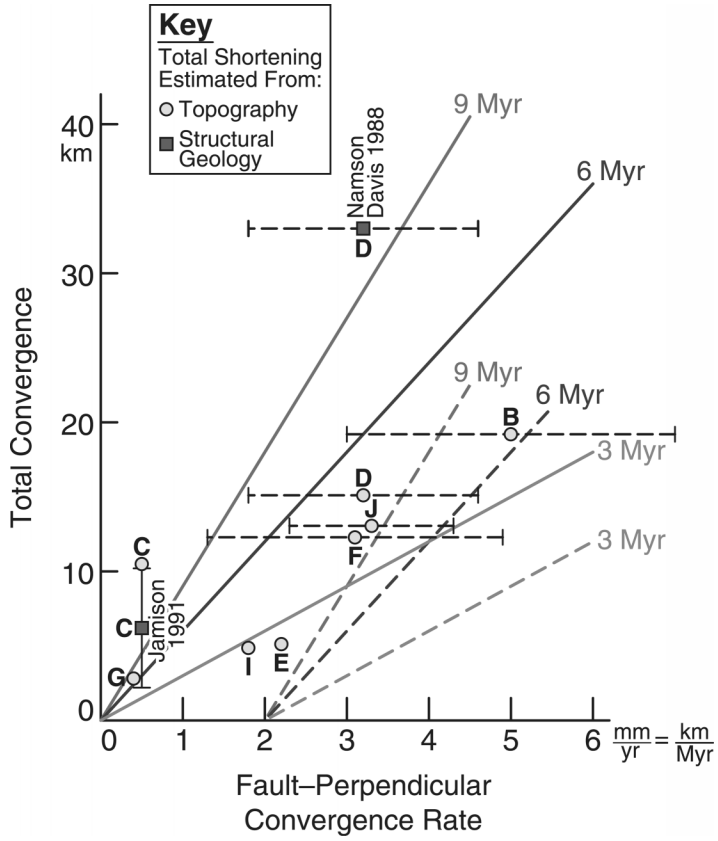

Figure 6. Convergence vs. fault-normal convergence rates. The minimum convergence (circles) across each of eight profiles is inferred from its elevation profile and a simple Airy model of isostatic compensation as discussed in the text. In addition, two convergence estimates (squares) from the structural geology of the Coast Range are shown: From a balanced cross section, Namson and Davis (1988) estimated 33 km of convergence on a profile near our profile D–D′. From the distribution and geometry of folds adjacent to the fault, Jamison (1991) estimated 6.0 ± 3.8 km of shortening normal to the San Andreas near our profile C–C′. The solid vertical bar shows these 95% confidence limits. Dashed horizontal bars show the 95% confidence limits on estimated fault-normal convergence rates for several profiles. Three solid lines emanating from the origin are isochrons corresponding to an assumed age (9 Ma, 6 Ma, or 3 Ma) for the onset of the Coast Range orogeny if erosion is neglected. The three dashed lines are similar isochrons except that a nominal erosion rate of 0.5 mm/yr was assumed.

Recent work aimed at dating the onset of the Coast Range orogeny is consistent with the greater age of onset indicated herein by the low rate of fault-normal convergence. The work has shown that the southern Diablo Range and the Temblor Range began their current phase of uplift by at least 5.4 Ma (Miller, 1998).

Any attempt to incorporate the effects of erosion will cause an increase in the estimated

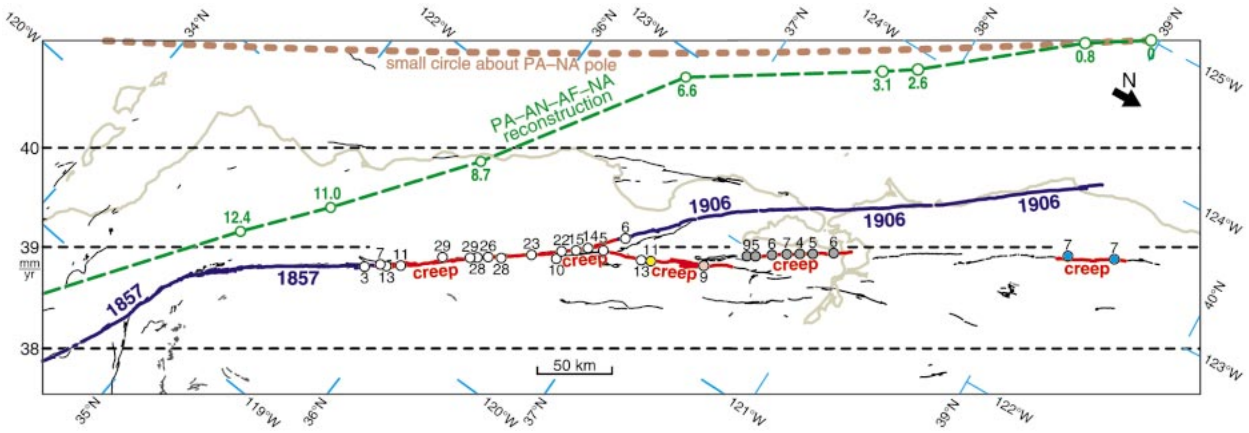

Figure 7. The 1857 and 1906 earthquake ruptures and fault segments with creep are compared with the direction of Pacific-Sierran plate motion. Circles filled various colors are places where the creep rate has been measured; adjacent numbers are speeds in mm/yr. The colors of the circles indicate the sources: white—Lisowski and Prescott (1981), yellow—Harsh and Burford (1982), pink—Oppenheimer et al. (1990), gray—Lienkaemper et al. (1991), blue—Galehouse (1996). The dotted red line is a small circle about the NUVEL-1A Pacific–North America pole of rotation (DeMets et al., 1994). The dashed green line shows the position of a point reconstructed with the Pacific plate relative to the North American plate from the present to ca. 15 Ma. Numerals give ages in millions of years of each reconstructed point. The Pacific–North America (PA-NA) rotations were found by summing (after appropriate interpolation) the Pacific-Antarctic (PA-AN) rotations of J. Stock (1997, personal commun., similar to those of Cande et al. [1995]), the Antarctica-Africa (AN-AF) rotations of Royer and Chang (1991), and the Africa–North America (AF-NA) rotations tabulated by Müller et al. (1991).

minimum time to build the ranges. As a specific example, we considered the case of a uniform rate of erosion along the ranges. We assumed a nominal rate of 0.5 mm/yr to obtain the set of dashed lines shown in Figure 6. In this case, all profiles indicate minimum durations of 6 m.y. or greater (Fig. 6).

PLATE RECONSTRUCTIONS, TIMING, AND GREAT BASIN DEFORMATION

Some prior analyses of plate reconstructions suggest that the main change in Pacific plate motion relative to North America occurred at ca. 3.5 Ma (Harbert and Cox, 1989; Harbert, 1991). Our own analysis of the plate-motion circuit using Pacific-Antarctic rotations provided by J. Stock (1997, personal commun.), similar to those used by Cande et al. (1995), indicates that the main change in Pacific–North America plate motion occurred at ca. 6.6 Ma (Fig. 7). This timing is consistent with the Pacific-Antarctic results of Cande et al. (1995), who found that the late Neogene change in motion consisted of an abrupt 8° change near 5.9 Ma superimposed on a more gradual change that began near 12 Ma. A more recent analysis of Pacific-Antarctic plate motion indicates that there was a 20°–25° change in Pacific–North America plate motion at ca. 8 Ma (Atwater and Stock, 1998). The change was progressive, taking several million years to occur, and was clearly pre-Pliocene in age (J. Stock, 1999, personal commun.). The minimum age of 3 Ma for the onset of the Coast Range orogeny that we infer from the minimum convergence needed to produce the topography of the ranges is consistent with the hypothesis that the orogeny was caused by a change in plate motion at 3 Ma or earlier. The minimum age of 7 Ma that we infer from the convergence estimated from balanced cross sections (Namson and Davis, 1988), however, is inconsistent with this timing but consistent with the current best estimates for the change in plate motion at 6.6 or 8 Ma.

The 20°–25° change in direction of plate motion strongly contrasts with the present angle of convergence (0.7°–4.7°) that we estimate across most sections of the San Andreas and related strike-slip faults (Table 2). Although the azimuth of sections of the San Andreas and related faults may have been altered in central California over the past 3–8 m.y., this difference in azimuth strongly suggests that the Sierran microplate must also have changed direction of motion by nearly as much as the change in Pacific plate motion relative to North America. Thus, the deformation in the Basin and Range, which accommodates motion between the Sierran microplate and the North American plate, must also have changed near 6.6 Ma or 8 Ma in response to the change in Pacific plate motion.

From geologic reconstructions of the central Basin and Range based on evidence independent of what we present here, Wernicke and Snow (1998) inferred a change of motion of the Sierran microplate relative to the Colorado Plateau. They found that motion changed from mainly westward motion exceeding 20 mm/yr between 16 and 10 Ma, to northwestward to north-northwestward motion at a rate of ~15 mm/yr since 8 to 10 Ma, a change that is similar, at least in sense, to that inferred here.

CREEPING VERSUS LOCKED SEGMENTS OF THE FAULT

Some sections of the San Andreas fault system rupture in large or great earthquakes, whereas other sections creep, rupture in small to moderate earthquakes, or both. The frictional force along a fault is proportional to the normal force across a fault. We reason that, all other factors being equal, the normal force should be greater where convergence rate across a fault is greater, and therefore so is the frictional resisting force. A low normal force may be conducive to stable sliding and a high normal force may be above the critical value for fault slip to be unstable (i.e., the fault is locked between large or great earthquakes) (Scholz, 1990). Here, we examine that hypothesis.

Figure 7 shows which sections of the fault appear locked between large or great earthquakes and which fail in creep, small to moderate earthquakes, or both. The creeping sections of the fault include the San Andreas

between Parkfield and San Juan Bautista, the Calaveras fault, the Hayward fault north of the Mission link, the Rodgers Creek fault, the Green Valley fault, the Maacama fault, and the Bartlett Springs fault (Lisowski and Prescott, 1981; Harsh and Burford, 1982; Oppenheimer et al., 1990; Lienkaemper et al., 1991; Galehouse, 1996). On first inspection, Figure 7 suggests a relationship between the strike of the faults, the direction of plate motion, and fault behavior. The creeping sections of the fault in nearly every case strike nearly parallel to the direction of relative plate motion (Fig. 7), i.e., the amount of inferred convergence is small (Table 2). Except for the short creeping section of the San Andreas fault north of the Calaveras junction, the creeping sections strike clockwise of, parallel to, or no more than 4.7° counterclockwise of the direction of plate motion (Table 2).

Moreover, some contrasts between locked and nonlocked sections stand out: substantial parts of the locked sections of faults have strikes 7°–32° counterclockwise of the direction of plate motion (i.e., along profiles A–A′, B–B′, E–E′, F–F′, and J–J′; Table 2). Across profiles E–E′ and F–F′ there is a strong contrast between the strike of the locked San Andreas (14.6° and 13.1°, respectively, counterclockwise of the direction of plate motion) and that of the Calaveras fault, which both creeps and slips in moderate earthquakes (8.4° and 3.3°, respectively, clockwise of the direction of plate motion).

Several aspects of Figure 7 and Table 2 weigh against our hypothesis, however, at least as the sole explanation for fault behavior. There are substantial sections of fault with small inferred rates of fault-normal convergence across which the San Andreas fault is locked. The two outstanding examples are the section between the big bend and Parkfield and the section from the Santa Cruz Mountains to Bodega Bay (e.g., the sections crossed by profiles C–C′, G–G′, H–H′, and I–I′). Perhaps their proximity to the highly convergent big bend and central California curving sections of the fault influence slip along them. Moreover, where the geometry of the fault system is simplest, i.e., between the Calaveras junction and the big bend, the creeping section of the San Andreas (i.e., the section between Parkfield and the Calaveras junction [Lisowski and Prescott, 1981; Burford and Harsh, 1980]) is the locus of greater convergence (3.2 $\pm$ 1.4 mm/yr across D–D′) than is the locked part of the fault (0.5 $\pm$ 1.8 mm/yr), which is south of Parkfield.

Thus, our hypothesis is at best a partial explanation for the observed distribution of locked and nonlocked sections of the fault. Undoubtedly, other factors are also important and perhaps much more important. For example, the nonlocked segments in central California occur where the faults regionally cut the upper plate of the Coast Range thrust. Where the Great Valley Formation is present above the Franciscan Formation, it may act as a hydraulic cap that helps to maintain high pore pressure caused by carbon dioxide produced in the underlying Franciscan rocks and to direct fluid flow into the fault (Irwin and Barnes, 1975).

CONCLUSIONS

The boundary between the Pacific plate and the Sierran microplate mainly accommodates convergent wrenching, but locally accommodates divergent wrenching, in particular in the northern San Francisco Bay area. The size of mountain ranges in the Coast Ranges tends to increase with increasing fault-normal convergence rate. If erosion is neglected, the cross-sectional areas of the mountains can have been produced at the present rates of fault-normal convergence in 3 to 6 m.y. In contrast, the amount of convergence inferred by Namson and Davis (1988) across the Diablo Range requires 7 to 18 m.y. at the present rates of fault-normal convergence, in contradiction to long-standing assumptions about the timing of the Coast Range orogeny. The present angle of convergence across the San Andreas and related faults is small relative to the change in direction of motion of the Pacific plate relative to the North American plate at 8 to 6 Ma. We infer that the Sierran microplate must also have changed motion to a more northerly direction relative to the North American plate at the same time as the change in Pacific plate motion. We are impressed by how much information about fault-normal convergence is contained in the strike of faults in the San Andreas system.

ACKNOWLEDGMENTS

We thank Bob Simpson for the use of his plotting program for digital topography and for his instructions on how to use it. The digitized representations of the faults shown in Figures 2, 3, and 6 were kindly made available to us by the California Division of Mines and Geology. We thank Joann Stock for supplying Pacific-Antarctic rotations and associated covariance matrices. We thank Tim Henstock, Tanya Atwater, Hans Avé Lallemant, Roland Bürgmann, Ray Weldon, and Joann Stock for helpful comments on various versions of the manuscript. Much of this work was performed at the Jet Propulsion Laboratory, California Institute of Technology, under contract with the National Aeronautics and Space Administration.

REFERENCES CITED

Argus, D.F., and Gordon, R.G., 1990, Pacific–North American plate motion from very long baseline interferometry compared with motion inferred from magnetic anomalies, transform faults, and earthquake slip vectors: Journal of Geophysical Research, v. 95, p. 17315–17324.

Argus, D.F., and Gordon, R.G., 1991, Current Sierra Nevada–North America motion from very long baseline interferometry: Implications for the kinematics of the western United States: Geology, v. 19, p. 1085–1088.

Argus, D.F., and Gordon, R.G., 1996, Tests of the rigid-plate hypothesis and bounds on intraplate deformation using geodetic data from very long baseline interferometry: Journal of Geophysical Research, v. 101, p. 13555–13572.

Argus, D.F., Peltier, W.R., and Watkins, M.M., 1999, Glacial isostatic adjustment observed using very long baseline interferometry and satellite laser ranging: Journal of Geophysical Research, v. 104, p. 29077–29093.

Atwater, T., and Stock, J., 1998, Pacific–North America plate tectonics of the Neogene southwestern United States: An update: International Geology Review, v. 40, p. 375–402.

Bennett, R.A., Davis, J.L., and Wernicke, B.P., 1998, Continuous GPS measurements of deformation across the northern Basin and Range province: Geophysical Research Letters, v. 25, p. 563–566.

Burford, R.O., and Harsh, P.W., 1980, Slip on the San Andreas fault in central California from alinement array surveys: Bulletin of the Seismological Society of America, v. 70, p. 1233–1261.

Cande, S.C., Raymond, C.A., Stock, J., and Haxby, W.F., 1995, Geophysics of the Pitman fracture zone and Pacific-Antarctic plate motions during the Cenozoic: Science, v. 270, p. 947–953.

Clark, T.A., Gordon, D., Himwich, W.E., Ma, C., Mallama, A., and Ryan, J.W., 1987, Determination of relative site motions in the western United States using Mark III very long baseline radio interferometry: Journal of Geophysical Research, v. 92, p. 12741–12750.

DeMets, C., and Dixon, T.H., 1999, New kinematic models for Pacific–North America motion from 3 Ma to present, I: Evidence for steady motion and biases in the NUVEL-1A model: Geophysical Research Letters, v. 26, p. 1921–1924.

DeMets, C., Gordon, R.G., Argus, D.F., and Stein, S., 1990, Current plate motions: Geophysical Journal International, v. 101, p. 425–478.

DeMets, C., Gordon, R.G., Argus, D.F., and Stein, S., 1994, Effect of recent revisions to the geomagnetic reversal time scale on estimates of current plate motion: Geophysical Research Letters, v. 21, p. 2191–2194.

Dixon, T.H., Robaudo, S., Lee, J., and Reheis, M.C., 1995, Constraints on present-day Basin and Range deformation from space geodesy: Tectonics, v. 14, p. 755–772.

Dixon, T.H., Miller, M., Farina, F., Wang, H.Z., Johnson, D., 2000, Present-day motion of the Sierra Nevada block and some tectonic implications for the Basin and Range province, North American Cordillera: Tectonics, v. 19, p. 1–24.

England, P., and Houseman, G., 1989, Extension during continental convergence, with application to the Tibetan Plateau: Journal of Geophysical Research, v. 94, p. 17561–17579.

Feigl, K.L., Agnew, D.C., Bock, Y., Dong, D., Donnellan, A., Hager, B.H., Herring, T.A., Jackson, D.D., Jordan, T.H., King, R.W., Larsen, S., Larson, K.M., Murray, M.M., Shen, Z., and Webb, F.H., 1993, Space geodetic measurement of the velocity field of central and southern California, 1984–1992: Journal of Geophysical Research, v. 98, p. 21677–21712.

Freymueller, J.T., Murray, M.H., Segall, P., and Castillo, D., 1999, Kinematics of the Pacific–North America plate boundary zone, northern California: Journal of Geophysical Research, v. 104, p. 7419–7441.

Fuis, G.S., and Mooney, W.D., 1990, Lithospheric structure and tectonics from seismic-refraction and other data, *in* Wallace, R., ed., The San Andreas fault system,

California: U.S. Geological Survey Professional Paper 1515, p. 207–236.
Furlong, K.P., 1993, Thermal-rheologic evolution of the upper mantle and the development of the San Andreas fault system: Tectonophysics, v. 223, p. 149–164.
Galehouse, J.S., 1996, Theodolite measurements of creep rates on San Francisco Bay region faults, *in* Natural hazards and earthquake research program annual project summaries: XXXVI: U.S. Geological Survey Open-File Report 95-210, p. 1103.
Gordon, D., Ma, C., and Ryan, J.W., 1993, Results from the CDP Mobile VLBI program in the western United States, *in* Smith, D.E., and Turcotte, D.L., eds., Contributions of space geodesy to geodynamics: American Geophysical Union Geodynamics Series, v. 23, p. 131–138.
Harbert, W., 1991, Late Neogene relative motions of the Pacific and North America plates: Tectonics, v. 10, p. 1–15.
Harbert, W., and Cox, A., 1989, Late Neogene motion of the Pacific plate: Journal of Geophysical Research, v. 94, p. 3052–3064.
Harsh, P.W., and Burford, R.O., 1982, Alinement array measurements of fault slip in the eastern San Francisco Bay area, California, *in* Hart, E.W., Hirschfeld, S.E., and Schulz, S.S., eds., Conference on earthquake hazards in the eastern San Francisco Bay area: California Division of Mines and Geology Special Publication 62, p. 251–260.
Irwin, W.P., and Barnes, I., 1975, Effect of geologic structure and metamorphic fluids on seismic behavior of the San Andreas fault system in central and northern California: Geology, v. 3, p. 713–716.
Jamison, W.R., 1991, Kinematics of compressional fold development in convergent wrench terranes: Tectonophysics, v. 190, p. 209–232.
Jennings, C.W., 1994, Fault activity map of California and adjacent areas: Sacramento, California Division of Mines and Geology, scale 1:750 000, 1 sheet.
Lienkaemper, J.J., Borchardt, G., and Lisowski, M., 1991, Historic creep rate and potential for seismic slip along the Hayward fault, California: Journal of Geophysical Research, v. 96, p. 18261–18283.
Lisowski, M., and Prescott, W.H., 1981, Short-range distance measurements along the San Andreas fault in central California, 1975 to 1979: Bulletin of the Seismological Society of America, v. 71, p. 1607–1624.
Lisowski, M., Savage, J.C., and Prescott, W.H., 1991, The velocity field along the San Andreas fault in central and southern California: Journal of Geophysical Research, v. 96, p. 8369–8389.
Ma, C., Ryan, J.W., and Caprette, D.S., 1994, NASA space geodesy program–GSFC data analysis—1993: VLBI geodetic results 1979–92: Greenbelt, Maryland, NASA Technical Memorandum 104605, 231 p.
McLaughlin, R.J., Sliter, W.V., Sorg, D.H., Russell, P.C., and Sarna-Wojcicki, A.M., 1996, Large-scale right-slip displacement on the east San Francisco Bay region fault system, California: Implications for location of late Miocene to Pliocene Pacific plate boundary: Tectonics, v. 15, p. 1–18.
Miller, D.D., 1998, Sequence stratigraphy and controls on deposition of the upper Cenozoic Tulare Formation, San Joaquin Valley, California [Ph.D. thesis]: Stanford, California, Stanford University, 179 p.
Minster, J.B., and Jordan, T.H., 1987, Vector constraints on western U.S. deformation from space geodesy, neotectonics, and plate motions: Journal of Geophysical Research, v. 92, p. 4798–4804.
Mount, V.S., and Suppe, J., 1987, State of stress near the San Andreas fault: Implications for wrench tectonics: Geology, v. 15, p. 1143–1146.
Müller, R.D., Sandwell, D.T., Tucholke, B.E., Sclater, J.G., and Shaw, P.R., 1991, Depth to basement and geoid expression of the Kane fracture zone: A comparison: Marine Geophysical Research, v. 13, p. 105–129.
Namson, J.S., and Davis, T.L., 1988, Seismically active fold and thrust belt in the San Joaquin Valley, central California: Geological Society of America Bulletin, v. 100, p. 257–273.
Niemi, T.M., and Hall, N.T., 1992, Late Holocene slip rate and recurrence of great earthquakes on the San Andreas fault in northern California: Geology, v. 20, p. 195–198.
Oppenheimer, D.H., Bakun, W.H., and Lindh, A.G., 1990, Slip partitioning of the Calaveras fault, California, and prospects for future earthquakes: Journal of Geophysical Research, v. 95, p. 8483–8498.
Page, B.M., 1984, The Calaveras fault zone of California, an active plate boundary element, *in* Bennett, J.H., and Sherburne, R.W., eds., The 1984 Morgan Hill California earthquake: California Division of Mines and Geology Special Publication 68, p. 109–122.
Page, B.M., and Engebretson, D.C., 1984, Correlation between the geologic record and computed plate motions for central California: Tectonics, v. 3, p. 133–155.
Prentice, C.S., 1989, Earthquake geology of the northern San Andreas fault near Point Arena, California [Ph.D. thesis]: Pasadena, California Institute of Technology, 252 p.
Royer, J.-Y., and Chang, T., 1991, Evidence for relative motions between the Indian and Australian plates during the last 20 Myr from plate tectonic reconstructions: Implications for the deformation of the Indo-Australian plate: Journal of Geophysical Research, v. 96, p. 11779–11802.
Sauber, J., Lisowski, M., and Solomon, S.C., 1989, Geodetic measurement of deformation east of the San Andreas fault in central California, *in* Cohen, S., and Vanicek, O., eds., Slow deformation and transmission of stress in the Earth: Washington, D.C., American Geophysical Union, Geophysical Monograph Series, p. 71–86.
Savage, J.C., Lisowski, M., and Prescott, W.H., 1990, An apparent shear zone trending north-northwest across the Mojave desert into Owens Valley, eastern California: Geophysical Research Letters, v. 17, p. 2113–2116.
Savage, J.C., Simpson, R.W., and Murray, M.H., 1998, Strain accumulation rates in the San Francisco Bay area, 1972–1989: Journal of Geophysical Research, v. 103, p. 18039–18051.
Scholz, C.H., 1990, The mechanics of earthquakes and faulting: Cambridge, U.K., Cambridge University Press, 439 p.
Sieh, K.E., and Jahns, R., 1984, Holocene activity of the San Andreas fault at Wallace Creek, California: Geological Society of America Bulletin, v. 95, p. 883–896.
Thatcher, W., Foulger, G.R., Julian, B.R., Svarc, J., Quilty, E., and Bawden G.W., 1999, Present-day deformation across the Basin and Range province, western United States: Science, v. 283, p. 1714–1718.
Ward, S.N., 1988, North America–Pacific plate boundary, an elastic-plastic megashear: Evidence from very long baseline interferometry: Journal of Geophysical Research, v. 93, p. 7716–7728.
Wernicke, B., and Snow, J.K., 1998, Cenozoic tectonism in the central Basin and Range: Motion of the Sierran–Great Valley block: International Geology Review, v. 40, p. 403–410.
Zoback, M.D., Zoback, M.L., Mount, V.S., Suppe, J., Eaton, J.P., Healy, J.H., Oppenheimer, D., Reasenberg, P., Jones, L., Raleigh, C.B., Wong, I.G., Scotti, O., and Wentworth, C., 1987, New evidence on the state of stress of the San Andreas Fault System: Science, v. 238, p. 1105–1111.

MANUSCRIPT RECEIVED BY THE SOCIETY MAY 28, 1999
REVISED MANUSCRIPT RECEIVED JANUARY 22, 2000
MANUSCRIPT ACCEPTED MAY 1, 2001

Printed in the USA